Journal of Applied Polymer Science

Wire-shaped, dye-sensitized solar cells with poly(vinyl alcohol) gel electrolyte and metal filaments

Ji Hyun Kwon, Jeong Soo Kim
Department of Polymer Science and Engineering, Chungnam National University, 99 Daehack-Ro, Daejeon 305-764, South Korea
Correspondence to: J. S. Kim (E-mail: jskim@cnu.ac.kr)

ABSTRACT: A kind of wire-shaped, dye-sensitized solar cell (WDSSC) composed of poly(vinyl alcohol) (PVA) gel electrolyte and filament-formed electrodes of titanium and platinum was prepared, and its photovoltaic performance was analyzed with the variations in the dimensions of the electrodes and cells. The dimensions of the wire-shaped cell were adjusted through the thickness of the TiO_2 layer, the amount of PVA gel electrolyte, and length of the Pt filament. The dominant parameters determining the cell performance were mainly analyzed with the results from the various scanning electron microscopy images and fitted plots of electrochemical impedance spectroscopy. Although the conversion efficiencies of the fabricated WDSSCs were relatively lower than those of the conventional dye-sensitized solar cells, this development should provide important guiding directions for the design of similar WDSSCs with higher efficiencies. © 2016 Wiley Periodicals, Inc. J. Appl. Polym. Sci. **2016**, *133*, 43439.

KEYWORDS: batteries and fuel cells; electrochemistry; polyelectrolytes

Received 6 October 2015; accepted 15 January 2016
DOI: 10.1002/app.43439

INTRODUCTION

Dye-sensitized solar cells (DSSCs) have received extensive attention because of their high energy conversion efficiency (η), low production cost, easy and diverse fabrication methods, and control of the absorption spectrum through the tuning of colors. To widen the application area of DSSCs, their diversity in shape and flexibility has been studied by many scientists. In general, a DSSC consists of transparent conducting glass, nanoporous high band-gap semiconductors such as TiO_2, sensitizing dye, a charge-transporting liquid electrolyte, and a metal (most frequently, platinum) counter electrode.[1] The driving force of photovoltaics in DSSC is the injection of electrons into the high band-gap semiconductors separated from the electron–hole pairs (excitons) of dyes generated through photon absorption. The electric current generated through the injected electrons out to an external circuit is possible with the shuttling characteristics of electrolytes, which are represented by iodide (I^-) and triiodide (I_3^-) ions in the electrolyte.[2,3]

However, a critical barrier to overcome for the variation in the shape of DSSCs is the liquid electrolyte itself, which results in its leakage and low volatility. To solve these problems, many efforts have been made to replace the liquid electrolyte with a solid or quasi-solid electrolyte, such as a polymer gel electrolyte, solid polymer electrolyte, or organic hole-transport material.[4] Polymer gel electrolytes are generally known to have some merits as ionic materials for electronic applications; these include good mechanical properties, light weight, variation in shape, and good contact with electrodes.[5] Among the polymer gel electrolytes that have frequently been used are poly(ethylene glycol), poly(propylene glycol), poly(vinylidene fluoride), and poly(vinyl alcohol) (PVA). The dissolution of a polymer electrolyte proceeds through coordinative interactions between the polar group of the polymer matrix and the ion of the metal salts.[6] Among the listed polymer matrices, PVA was selected in this study because it is known to form a complex with iodide and to have good retention properties of solvent, use in a wide temperature range, and a nontoxic nature.[7]

The main reasons why wire-shaped dye-sensitized solar cells (WDSSCs) have attracted a lot of attention are their module flexibility and the possibility of a low price, light weight, and diverse selectivity in the electrode materials. Additionally, if it is fabricated in three-dimensional form, the active area of the module can be expanded, and the dependence of the irradiation angle of light can be decreased. Moreover, with metal wire as an electrode, WDSSCs can also attain flexibility, expansibility, and better conductivity.[8]

In this study, a WDSSC was manufactured with titanium and platinum filaments with a PVA gel electrolyte to improve the limits of the liquid electrolyte and conventional DSSC. The photovoltaic and electrochemical performances were analyzed in terms of the length and diameter of the Pt filament, the thickness of the PVA gel electrolyte, and the number of TiO_2 layers.

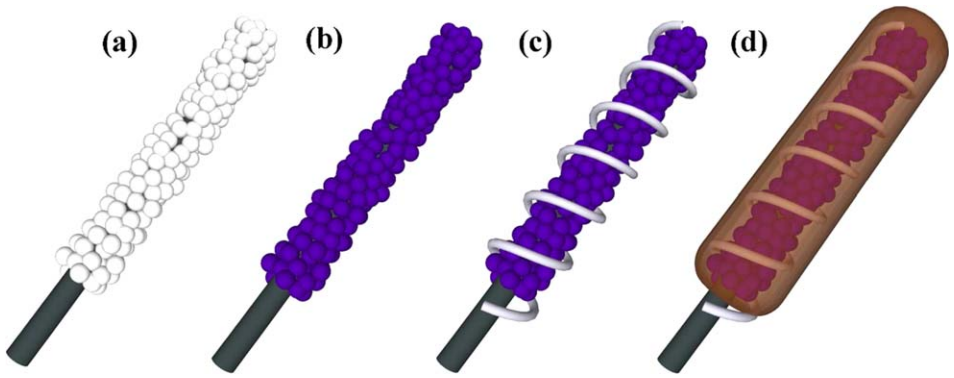

Figure 1. Schematic presentation of the fabrication steps of the WDSSCs: (a) TiO_2 sintering, (b) N3 dye absorption, (c) Pt filament winding, and (d) coating of the PVA gel electrolyte. [Color figure can be viewed in the online issue, which is available at wileyonlinelibrary.com.]

In this study, we were not aiming to attain a high-performing, wire-shaped solar cell but to analyze the shape factors of wire-shaped solar cells that are important in determining their performance.

EXPERIMENTAL

Materials

A titanium filament with a diameter of 500 μm and two kinds of platinum filaments with diameters of 100 μm (Pt-100) and 250 μm (Pt-250) were purchased from Alfa Aesar and Ill-Dong Chem. TiO_2 powder (Degusa P25), ethanol (Samchun), acetyl acetone (99.0%, Samchun), Triton X-100 (Duksan), and *cis*-di(thiocyanato)-*bis*[2,2′-bipyridyl-4,4′-dicarboxylic acid] ruthenium(II) (N3; Solaronix SA) were used to prepare the anode. PVA (weight-average molecular weight = 500, Samchun), potassium iodide (KI; Duksan), iodine (99.8%, Sigma), and 1-methyl-2-pyrrolidinone (>99%, Alfa Aesar) were used for the polymer gel electrolyte. All chemicals were used without purification.

Preparation of the TiO_2 Multilayer

To prepare the anode, the TiO_2 paste was prepared first through the blending of 6 g of P25 TiO_2, 20 mL of ethanol, 2 mL of acetyl acetone, and 2 drops of Triton X-100. The Ti filament was cleaned with acetone in an ultrasonic bath for 5 min and coated with the prepared TiO_2 paste by a dip coater (EF-4200). The Ti filament coated with the TiO_2 paste was sintered at 450 °C for 30 min and then allowed to cool to room temperature. The thickness of the TiO_2 multilayer surrounding the Ti filament was controlled by the number of immersions into the TiO_2 paste with the Ti filament with the sintering cycles.

Dye Adsorption and Analysis of the Amount

The prepared electrode was immersed in a solution of N3 dye (5×10^{-4} mol/L in absolute ethanol) for 24 h at room temperature. To remove the excess dye, the Ti filament was washed in ethanol, and a sequential drying process was performed. To measure the amount of adsorbed dye, the electrode was immersed into a 0.1*M* NaOH solution in a mixture of water and ethanol (volume ratio = 1:1) for 10 min. The concentration of desorbed solution of the N3 dye was measured by fitting to a calibration curve made with known concentration of dyes through an ultraviolet–visible (UV–vis) spectrophotometer (S-3100). The surface density of the adsorbed N3 dye was analyzed with the maximum absorbance at 535 nm and the thickness of the TiO_2 layers.

Preparation of the PVA Gel Electrolyte

The gel electrolyte was composed of KI, I_2, PVA as a polymer matrix, and *N*-methyl pyrrolidone as polar diluent. The molar ratio of the monomeric repeating unit of PVA to KI was fixed at 20. The weight ratio of KI to I_2 was 10. Two steps were required to prepare the PVA gel electrolyte. First, a 5.238-g mixture of PVA and KI was dissolved in 10 mL of N-methyl-2-pyrrolidone (NMP) at 200 °C for 2 h. Second, 0.1 g of I_2 was added to this solution, and the mixture was stirred continuously until the solution entered a homogeneous state at 150 °C. However, the thickness of the PVA gel electrolyte was controlled by the variation of the coating speed of the dip coater. The adjusted speed of the dip coater was set in the range 0.2–1.2 mm/s with 0.2 mm/s intervals. The macroscopic shape of the multilayer was observed with a scanning electron microscope (JSM-7000F, JEOL).

Fabrication of the WDSSCs

Figure 1 shows a schematic presentation of the WDSSC fabrication steps. The WDSSCs in this study were fabricated by the direct manual twisting of the sintered coaxial Ti/TiO_2 anodic electrodes with Pt cathodic electrodes; this was followed by their immersion into the gel electrolyte with a controlled dip coater. The performances of the prepared WDSSCs were evaluated under 1 sun (AM1.5) illumination with a solar simulator (PEC-L01). The photocurrent–voltage curves were recorded with an Ivium apparatus (IVIUMSTAT). The active length of the cell was adjusted to 2 cm. The active area of the cell was calculated by multiplication of the active length and diameter of the Ti filament, which gave a value of 0.1 cm^2.

Photovoltaic Performance Analysis of the WDSSCs

The photocurrent–voltage curves recorded in Ivium were analyzed in terms of η with the following equation and a calibration of the active area of the cell of 0.1 cm^2:

$$\eta\ (\%) = \mathrm{FF}\frac{V_{OC}J_{SC}}{P_{\mathrm{in}}} \times 100 \quad (1)$$

where V_{OC} is the open-circuit voltage (V), J_{SC} is the short-circuit current density (mA/cm^2), and P_{in} is the incident light

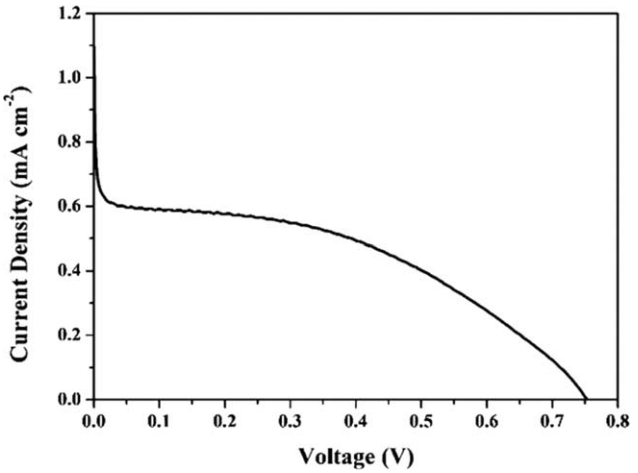

Figure 2. Example of typical raw current–voltage curves of WDSSCs fabricated with Pt-100, one layer of TiO_2, a dip-coating speed of 0.8 mm/s, and a 65 mm long Pt cathode.

intensity (mW/cm^{-2}). The fill factor (FF) was calculated with eq. (2):

$$FF = \frac{V_{max} J_{max}}{V_{OC} J_{SC}} \quad (2)$$

where V_{max} and J_{max} are the voltage and current density, respectively, obtainable at the maximum power point.

For detailed information on the photovoltage drop and charge trap, electrochemical impedance spectroscopy (EIS) was obtained and analyzed with an amplitude of 10 mV and a frequency range from 100 kHz to 0.1 Hz. The impedance measurement was carried out by the adaptation of V_{OC} as the bias voltage. The obtained plots were fitted with ZView software.

RESULTS AND DISCUSSION

Figure 2 shows a typical current-voltage (J–V) curve of the fabricated WDSSCs of this study; it shows an S-formed curve of higher current at a near-zero applied voltage. The form of the J–V curve varied by shunt resistance (R_{SH}) and series resistance (R_S).[9] R_S is related to the structure and junction of electrodes. R_{SH}, as a parallel resistance in solar cells, is usually added to explain the back transfer of electrons, which affects the cell performance through current dissipation caused by the recombination of electrons.[10] An increase in electron recombination should mean a decrease in the recombination resistance at the TiO_2/electrolyte interface (R_2) and R_{SH}; this eventually caused a decrease in the cell performance. The S-formed curves shown in this study were mostly resulted from an increase in R_S caused by the use of the polymer electrolyte.[11] The polymer chain mobility is usually much lower than that of a molecule of liquid electrolyte. In addition, the diameter of the TiO_2 nanoparticles was about 20 nm; this was comparable with the hydrodynamic volume of the swelled polymer. Therefore, it is difficult for the electrolyte to penetrate to the bottom of the TiO_2. The restoration of the oxidized dye was interrupted because of the slow transportation of ion in electrolyte.[4,12] Therefore, all of the values J_{SC} were calibrated in this study by the extrapolation of the curve to the decreasing portions of the current axis. The gap of calibrated values from raw J_{SC} had a tendency to increase in

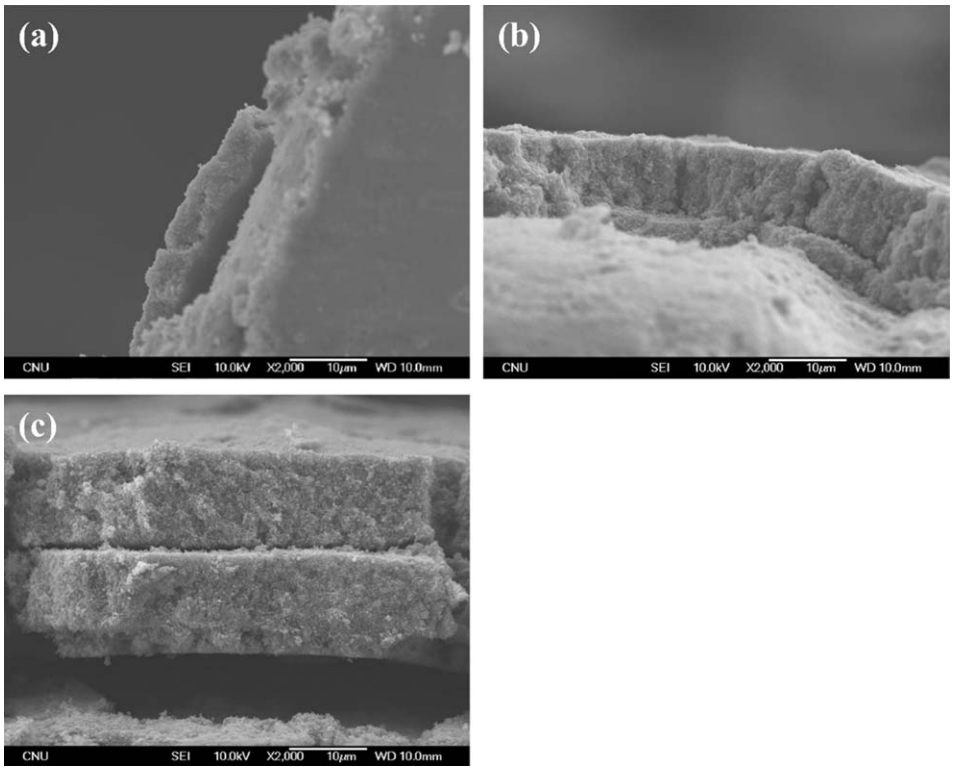

Figure 3. Cross-sectional SEM images of a Ti filament surrounded with different numbers of TiO_2 layers: (a) one layer, (b) two layers, and (c) three layers.

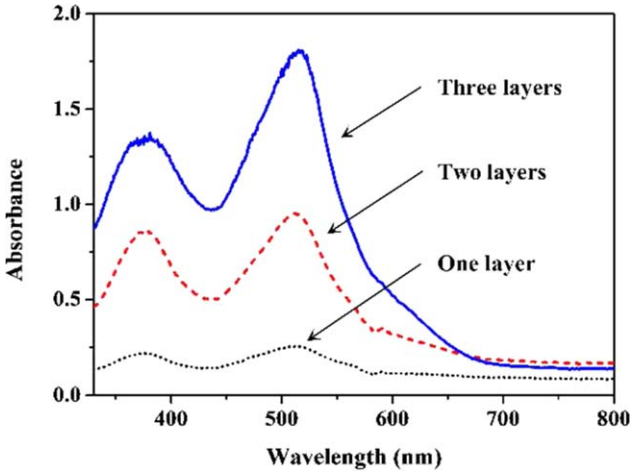

Figure 4. UV–vis absorption spectra of an aqueous extraction solution of 0.1*M* NaOH containing desorbed dye from the TiO_2 layers. [Color figure can be viewed in the online issue, which is available at wileyonlinelibrary.com.]

proportion to the numbers of TiO_2 layers; these values were 0.05, 1.82, and 3.37 mA cm^{-2} in accordance with one, two, and three layers, respectively, of TiO_2. These phenomena resulted from the penetration of the PVA gel electrolyte becoming more difficult as the number of TiO_2 layers increased.

Effect of the Numbers of TiO_2 Layers

Figure 3 shows the scanning electron microscopy (SEM) images of the TiO_2 multilayer with different numbers of coating layers on the Ti filament. The thickness and number of TiO_2 layers increased with repeated coatings and sintering. Additionally, the amount of adsorbed dye increased in relation to the thickness of the layer; those differences in the absorption intensity are clearly shown in the UV–vis absorption spectra in Figure 4. Table I summarizes the analyzed results of the thickness and dye adsorption. The thickness of TiO_2 increased from 4.75 to 25.86 μm, and the amount of adsorbed dye increased from 0.01×10^{-8} to 0.94×10^{-8} mol/cm^2 with increasing number of TiO_2 layers. These correlations were assumed to be caused by the fact that the surface area for dye loading increased with increasing number of TiO_2 layers; this increased the amount of dye adsorbed.

A series of WDSSCs was fabricated to study the effect of the TiO_2 layer, in which the Pt filament was always 65 mm long, and the PVA gel electrolyte was coated at a constant speed of 0.8 mm/s.

Table I. Variation in the Thickness of the TiO_2 Layers and the Amount of Adsorbed Dye on the Layers with the Number of Coating Cycles

Number of coating cycles	Layer thickness (μm)	Amount of adsorbed N3 dye (10^{-8} mol/cm^2)
1	4.75	1.05
2	14.63	8.05
3	25.86	31.4

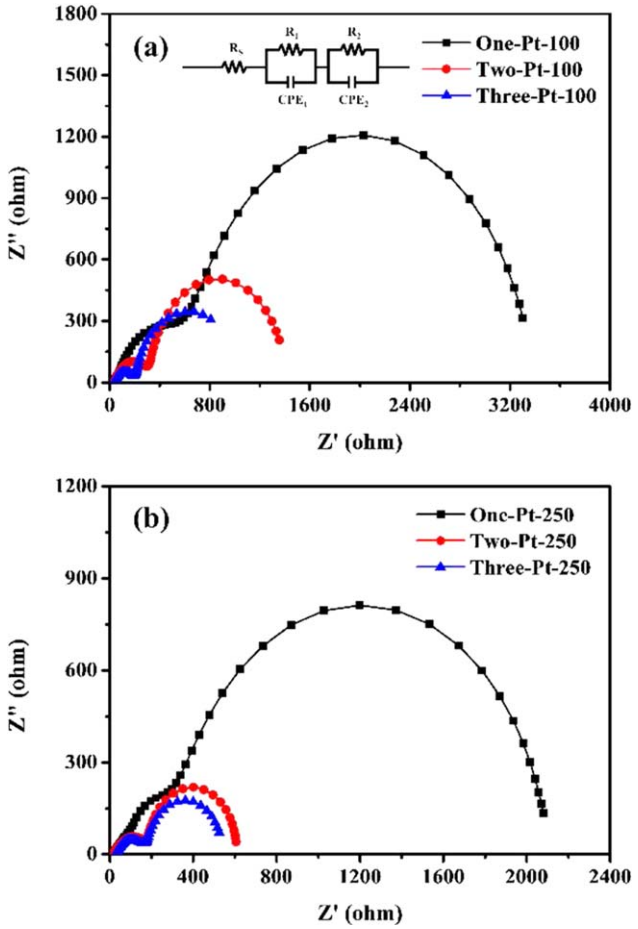

Figure 5. Nyquist plot of the WDSSCs under dark conditions with a −0.8-V bias on EIS according to the diameter of the Pt cathode and the number of coating cycles (denoted by the numerals in the sample codes): (a) Pt-100 and (b) Pt-250. The inset is an equivalent circuit for the WDSSCs. [Color figure can be viewed in the online issue, which is available at wileyonlinelibrary.com.]

Figure 5 shows the EIS spectra of the prepared WDSSCs obtained at a frequency range from 100 kHz to 0.1 Hz with different TiO_2 thicknesses. Their numerical data are shown in Table II. Two semicircles were consistently obtained by curve fitting. It is known that the starting point of the first semicircle is R_S. Additionally, the first semicircles at high frequency denote the charge-transfer resistance of the counter electrode to the electrolyte and contact resistance at the Ti/TiO_2 interface (R_1). On the other hand, second semicircles at low frequency denote R_2.[13] As shown in Table II, the R_S values of the WDSSCs increased with increasing thickness of the TiO_2 layers, regardless of the diameter of the Pt filament. On the contrary, the values of R_1 and R_2 showed a tendency to decrease with increasing thickness of the TiO_2 layers. An increase in R_S accompanying the thickness of TiO_2 is a common phenomenon resulting from the increase in the electron path length to the anodic electrode accompanying a serial resistance.[14] The inverse proportional decrease in R_1 to the thickness of TiO_2 is usually explained by contact improvement attained through the dense forming interface of the Ti filament and TiO_2 layer. The improved interfacial

Table II. Variation of the Fitted Parameters of EIS According to the Diameter of the Pt Filament and the Number of Coating Cycles

Pt filament	Number of coating cycles	R_S (Ω)	R_1 (Ω)	R_2 (Ω)
Pt-100	1	37.5	580	2740
	2	39.5	250	1100
	3	40.8	152	669
Pt-250	1	17.0	303	1670
	2	19.2	151	417
	3	29.5	135	359

adhesion is attained by the repeated heat treatment and compact packing of TiO_2; this eventually leads to a reduction in the charge transfer.[15] Electrons injected into the TiO_2 layers can combine with oxidized dye or oxidized ions (I_3^-) in the electrolyte. The reduction in R_2 means that the recombination of electrons can easily occur at the TiO_2/electrolyte interface.[16] A decreased R_2 with increasing number of TiO_2 layers occurred because the multilayer TiO_2 supplied more recombination sites to the electrons than the monolayer TiO_2 did.

Figure 6 shows the dependence of the main photovoltaic parameters of the fabricated WDSSCs on the increasing number of TiO_2 layers. With increasing number of TiO_2 layers from one to three, the J_{SC} values of the WDSSCs increased from 0.74 to 0.89 mA cm^{-2} in the case of Pt-100 and from 1.03 to 1.97 mA cm^{-2} in the case of Pt-250. The increasing J_{SC} in this case was caused by the increased amount of adsorbed dye; this eventually increased the efficiency of the light harvesting of WDSSC.[10] The thicker TiO_2 layer provided more sites for the adsorption of dye and a higher light-harvesting efficiency.[12]

However, the dependence of V_{OC} on the numbers of TiO_2 layers showed a different tendency from J_{SC}. V_{OC} is known to be related to the difference between the Fermi level of the semiconductor and the redox potential of the electrolyte. The concentration of electrons in the conduction band of TiO_2 consequently affects V_{OC}. Although V_{OC} of the WDSSCs with two layers of TiO_2 was higher than that with one layer, V_{OC} with three layers fell again to a value lower than that with two layers. It has been reported that the optimum thickness of TiO_2 in the usual platform DSSC is in the range 10–15 μm.[14,17] The increasing V_{OC} in the cells of the two-layer TiO_2 was caused by the increasing amount of injected electron into the conduction band of TiO_2. However, the decreasing V_{OC} in the three-layer cells could be explained by the aspect of the longer path length of electron transfer. The increasing electron combinations with the longer path length of the electron transfer to the anode led to a reduction in the electron concentration in the conduction band of TiO_2; this resulted in the reduction in the Fermi level of TiO_2 and the eventual reduction in V_{OC}.[1] This result matched well with the following eq. (3)[18]:

$$V_{OC} = \left(\frac{kT}{e}\right) \ln\left(\frac{I_{inj}}{n_{cb} k_{et} [I_3^-]}\right) \quad (3)$$

where I_{inj} is the charge flux from dye-sensitized electron injection, n_{cb} is the concentration of electrons in TiO_2, and k_{et} is the rate constant for triiodide reduction. In this study, the decrease in V_{OC} in the cells of three-layer TiO_2 could be also explained by the electron recombination at the TiO_2/electrolyte interface.

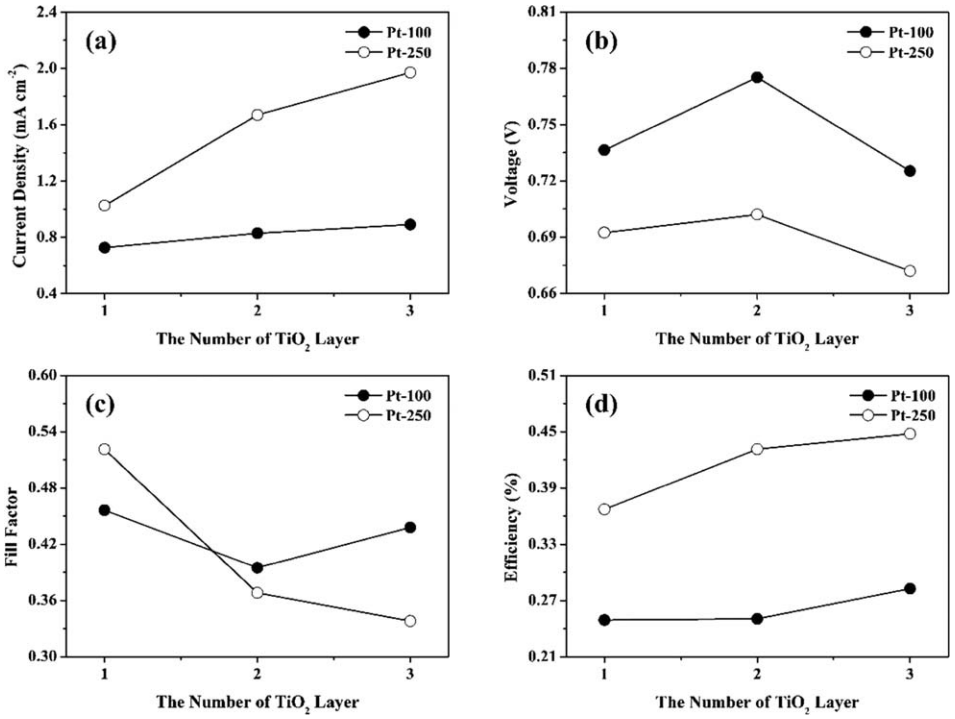

Figure 6. Variation of the photovoltaic parameters according to the number of TiO_2 layers: (a) J_{SC}, (b) V_{OC}, (c) FF, and (d) η.

Table III. Variation of the Fitted Parameters of EIS According to the Length of the Pt Filament

Pt filament	Length (mm)	R_S (Ω)	R_1 (Ω)	R_2 (Ω)
Pt-100	25	105.8	612.8	3585
	35	84.3	577.2	3405
	45	63.9	606.4	3409
	55	48.4	568.3	2939
	65	31.3	509.8	2839
Pt-250	25	77.9	388.9	3214
	35	52.0	319.4	2224
	45	30.9	286.8	2712
	55	24.6	235.8	2123
	65	17.7	232.0	2135

The FF of solar cells is known to be dependent on the internal resistance, including both R_{SH} and R_S. It is known that a decrease in R_{SH} and an increase in R_S reduce FF and the power conversion efficiency.[10] A decrease in FF accompanying an increase in the number of TiO_2 layers resulted from falling R_{SH} and rising R_S in the WDSSCs. The falling R_{SH} was caused by the increase in the recombination sites of electrons, and the rising R_S was caused by the increasing path length for electron transfer. On the other hand, the increasing power conversion efficiency accompanying the incremental increase in TiO_2 layers was caused by the increased amount of photosensitizing dye molecules.

Effect of the Length of the Pt Filament

Another series of WDSSCs was fabricated to study the effect of the length of the Pt filament. They were all fabricated with the anodes coated with one layer of TiO_2 and after the dip coating of the PVA gel electrolyte with a speed of 0.8 mm/s. Table III summarizes the fitted EIS parameters with the variation in the diameter and length of the Pt filament. With the lengthening of the Pt filament from 25 to 65 mm, the R_S values of the WDSSCs decreased rapidly from 105.8 to 31.3 Ω in the case of Pt-100 and from 77.9 to 17.7 Ω in the case of Pt-250. Furthermore, the values of R_1 and R_2 had a tendency to decrease with the lengthening of the Pt filament. The R_S was related to the sheet resistance of the counter electrode, the resistance of electrolyte, and the resistance of the photoanode (TiO_2).[19] The reduction in R_S was caused by the expansion in the surface area accompanying the lengthening of the Pt filament because the other fabrication conditions were all the same. The lengthening of Pt filament additionally resulted in decreases in R_1 and R_2. The largest portion of R_1 was the charge-transfer resistance for the reduction of triiodide at the electrolyte/Pt electrode interface. As a cathodic electrode, Pt provided additional catalytic activity for the reduction of the triiodide. Therefore, the decrease in R_1 resulted from the increase in the surface area responsible for the catalytic activity; this was proportional to the length of the Pt filament.[20,21] The increasing length of the Pt filament shortened the distance between the twisted counter electrode and accompanied the reduction in the ion-diffusion distance.[18] Therefore, the recombination rate of electrons increased because it helped the movement of ions along the narrowed electrode.

Figure 7 shows the variation of the photovoltaic parameters of the prepared WDSSCs, which was dependent on the length of the Pt filament. The J_{SC}, FF, and efficiency of the cells with Pt-100 and Pt-250 increased proportionally with the lengthening of the Pt filament from 25 to 65 mm. The increasing J_{SC} was

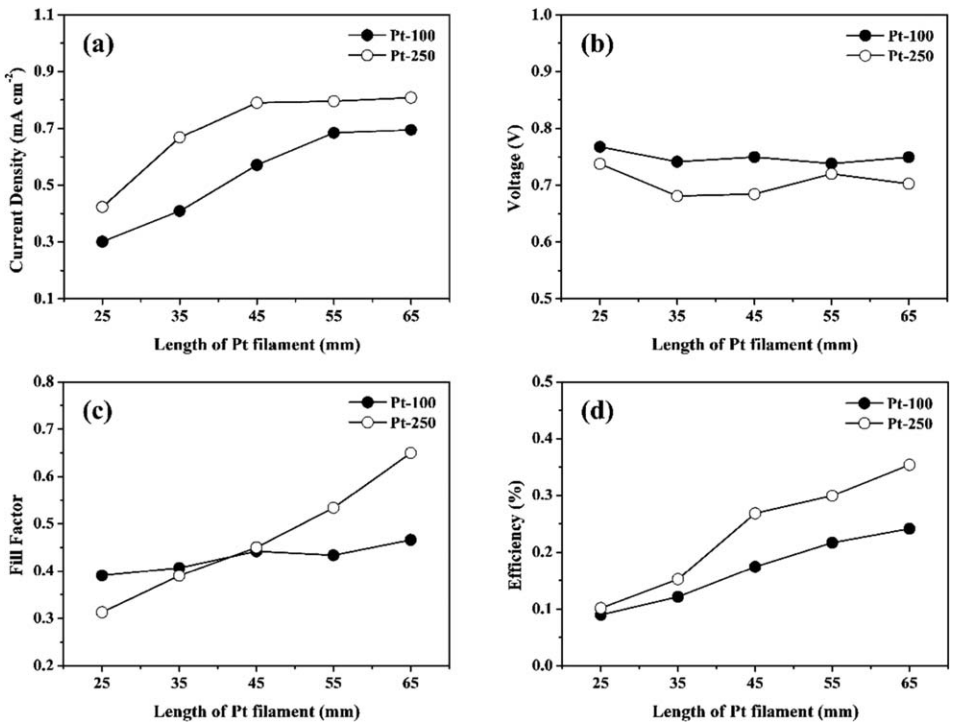

Figure 7. Variation of the photovoltaic parameters according to the length of the Pt filament: (a) J_{SC}, (b) V_{OC}, (c) FF, and (d) η.

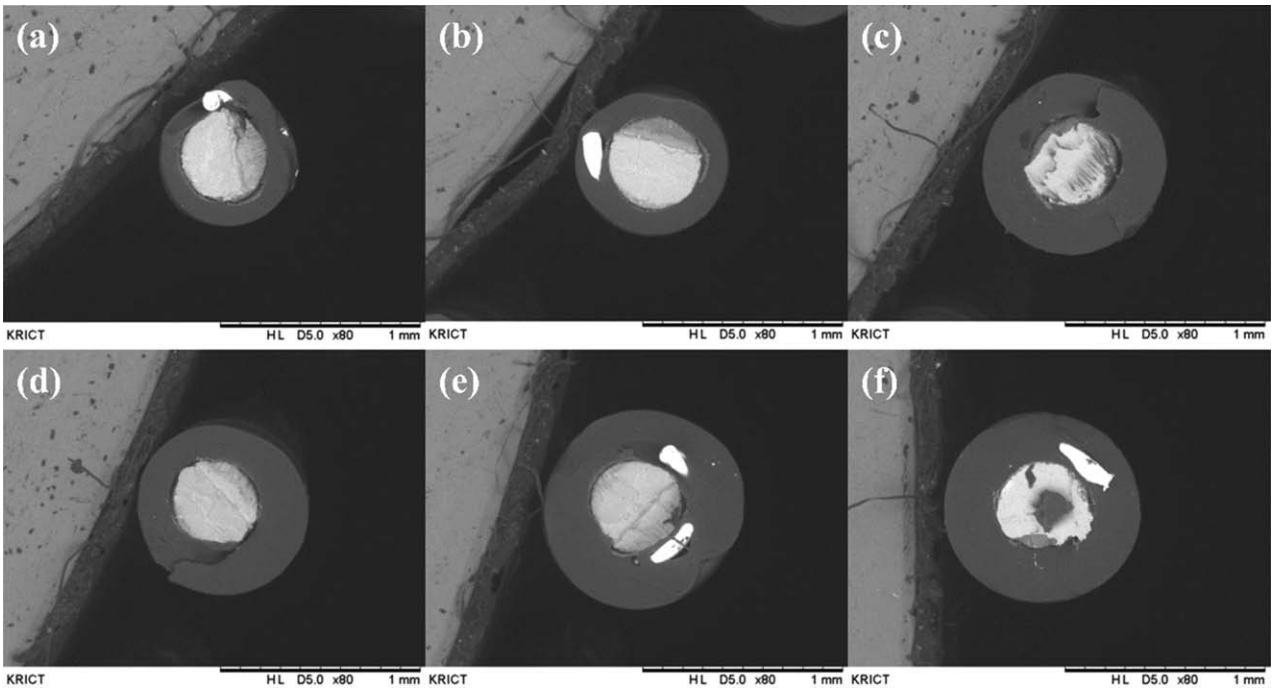

Figure 8. Cross-sectional SEM images of the WDSSCs showing the thickening of the PVA gel electrolyte with an increasing dip-coating speed on Pt-100: (a) 0.2, (b) 0.4, (c) 0.6, (d) 0.8, (e) 1.0, and (f) 1.2 mm/s.

caused by the lowered R_1 value, which was accompanied by the increase in the surface area of Pt; this means that electron transfer from the Pt electrode to the triiodide ion in the electrolyte became easier.[22] However, the values of V_{OC} stayed almost constant; this resulted from the unremarkable change in the Fermi level. The FF increase also accompanied the lengthening of the Pt filament from 0.39 to 0.47 in the case of Pt-100 and from 0.31 to 0.65 in the case of Pt-250. Through the data of EIS, the increasing diameter of Pt was shown to result in a decrease in R_2; this indicated an increasing electron recombination, decreasing R_{SH}, and decreasing FF. Despite the decreasing R_{SH}, as analyzed from EIS, this increasing FF was assumed to occur

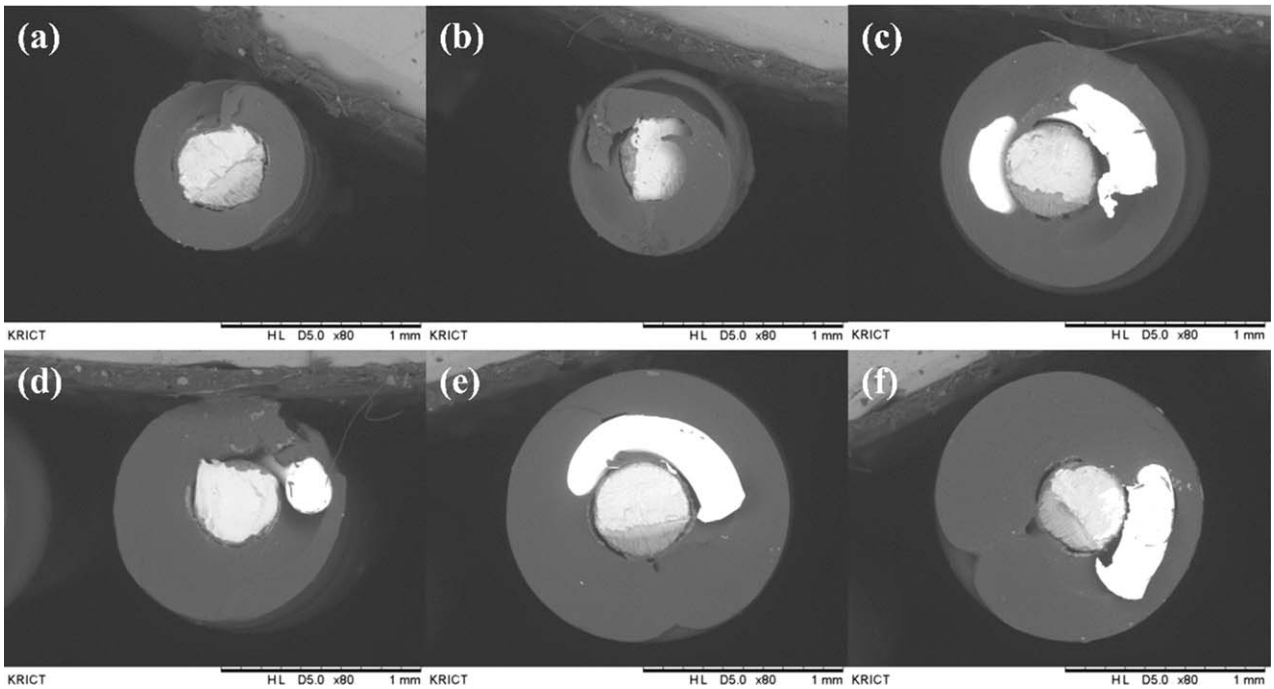

Figure 9. Cross-sectional SEM images of the WDSSCs showing the thickening of the PVA gel electrolyte with an increasing dip-coating speed on Pt-250: (a) 0.2, (b) 0.4, (c) 0.6, (d) 0.8, (e) 1.0, and (f) 1.2 mm/s.

Table IV. Variation of the Fitted Parameters of EIS According to the Diameter of the Pt Filament and the Coating Speed of the PVA Gel Electrolyte

Pt filament	Coating speed (mm/s)	Thickness (mm)	R_S (Ω)	R_1 (Ω)	R_2 (Ω)
Pt-100	0.2	0.11	53.2	333.7	3113
	0.4	0.13	36.3	458.2	2979
	0.6	0.21	36.5	515.5	2896
	0.8	0.22	33.3	533.3	2794
	1	0.27	39.3	521.8	2791
	1.2	0.26	45.7	531.5	3206
Pt-250	0.2	0.18	25.7	279.7	1251
	0.4	0.23	29.7	361.0	1987
	0.6	0.35	37.8	398.5	2381
	0.8	0.36	29.4	439.7	1387
	1	0.46	34.8	465.4	2067
	1.2	0.44	38.2	468.0	2610

because the decrease in R_S was the most dominant factor aroused through the lengthening of the Pt filament among all three factors (i.e., R_2, R_{SH}, and R_S).[23] The conversion efficiencies also consequently increased because they were a combined result of increasing J_{SC} and increasing FF with an almost constant V_{OC}. Therefore, this increase in η was fundamentally based on the decrease in the ion-diffusion path and the increase in the catalytic surface accompanying the increases in the diameter and length of the Pt filament.[18]

Effect of the Coating Speed of the PVA Gel Electrolyte

Figures 8 and 9 show the cross-sectional SEM image of WDSSCs with different coating speeds of the PVA gel electrolyte. An additional series of WDSSCs was fabricated to study the effect of the coating speed of the PVA gel electrolyte. These WDSSCs each had an anode of one-layer TiO_2 and a 65-mm Pt cathode filament. As shown in Table IV, the thickness of the gel electrolyte usually increases in proportion to the speed of dip coating, which reached a thickness plateau value for both Pt-100 and Pt-250. Their coating speeds were shown to be about 1.0 mm/s. Additionally, the smoothness of the coating electrolyte was observed to be best at 0.8 mm/s, although this was determined with the naked eye.

Table IV shows the fitted parameter of EIS, which was dependent on the dip-coating speed of the PVA gel electrolyte. The remarkable tendency exhibited in Table IV was the increase in the charge-transfer resistance (R_1); this accompanied the increase in the electrolyte thickness and resulted in an increase

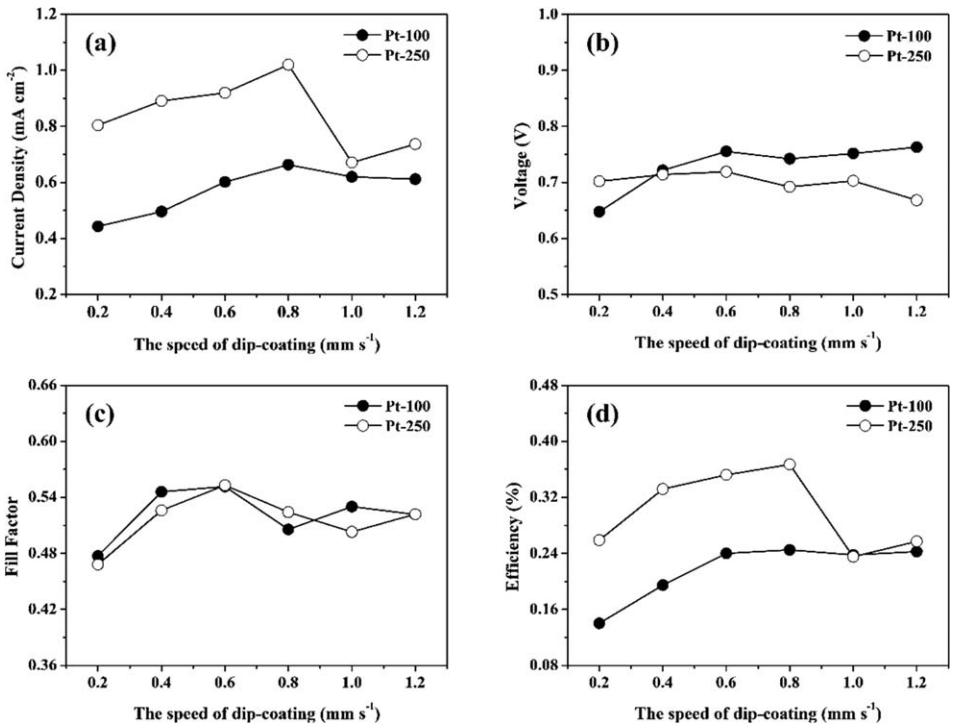

Figure 10. Variation of photovoltaic parameters according to the speed of dip coating: (a) J_{SC}, (b) V_{OC}, (c) FF, and (d) η.

in the redox species, polymer matrices, and a barrier to charge transfer. Figure 10 shows the photovoltaic parameters of the WDSSCs and their dependency on the coating speed of the PVA gel electrolyte. J_{SC} and η increased with increasing thickness of the electrolyte. Although we could not describe any clear tendency from the curves of Figure 9, we observed that the best photovoltaic performance was attained at a dip-coating speed of 0.8 mm/s; this was tentatively assumed to have resulted from the homogeneous and smooth surface of the coating layer.

Effect of the Diameter of the Pt Filament

Through the combination of data in Tables (II–IV), a common result was obtained. The resistance of the WDSSCs with Pt-250 was always less than that with Pt-100. The reason for this result could be described through the following Van der Pauw equation:

$$R_{SH} = \frac{\rho}{t} \quad (4)$$

where ρ is the resistivity and t is the thickness of the electrode. Because the resistivity of the Pt electrode was the same, the sheet resistances of the WDSSCs having Pt-250 with a larger diameter were lower than those of the WDSSCs having Pt-100 with a smaller one. Through the combination of the value of EIS data and the tendencies of Figure 9, the higher conversion efficiencies in the case of Pt-250 almost resulted from the higher values of J_{SC} because the values of V_{OC} and FF did not vary much, regardless of the diameter of Pt filament. The higher J_{SC} values were assumed to be caused eventually by the expansion of the contacting surface area of the cathode and the shortened path of triiodide diffusion accompanying the increase in its diameter.[18]

CONCLUSIONS

WDSSCs were successfully fabricated with PVA gel electrolyte with an abnormal supporting anode of Ti filament and a cathode of Pt filament. The thickness of the TiO_2 layers surrounding the Ti filament could be controlled and reached an optimum value to balance the increasing R_S. The increased contacting interface resulted from the increasing diameter and extending length of the Pt filament and usually led to an increase in the cell performance, which was caused by the increase in the short current density. The thickening of the gel electrolyte layer with a uniform surface was also important in increasing the performance of the WDSSCs. Although the WDSSCs fabricated in this study showed much lower performances as a kind of photovoltaic cells, and the analyzed results supply important considerations for designing similar types of photovoltaic cells.

ACKNOWLEDGMENTS

This research was supported by the Basic Science Research Program of the National Research Foundation of Korea, which is funded by the Ministry of Education, Science, and Technology (contract grant number 2010-0010045).

REFERENCES

1. Song, D. M.; Qiang, Y. H.; Zhao, X. Q.; Song, C. B. *Appl. Surf. Sci.* **2013**, *277*, 53.
2. Aziz, M. F.; Noor, I. M.; Sahraoui, B.; Arof, A. K. *Opt. Quant. Electron.* **2014**, *46*, 133.
3. Baglio, V.; Girolamo, M.; Antonucci, V.; Aricò, A. S. *Int. J. Electrochem. Sci.* **2011**, *6*, 3375.
4. Kang, M. S.; Kim, J. H.; Kim, Y. J.; Won, J.; Park, N. G.; Kang, Y. S. *Chem. Commun.* **2005**, *7*, 889.
5. Awadhia, A.; Agrawal, S. L. *Solid State Ionics* **2007**, *178*, 951.
6. Ahn, S. H.; Kim, H. W.; Lee, S. H.; Chi, W. S.; Choi, J. R.; Shul, Y. G.; Kim, J. H. *J. Chem. Eng.* **2011**, *28*, 138.
7. Bhad, S. N.; Sangawar, V. S. *Chem. Sci. Trans.* **2012**, *1*, 653.
8. Zou, D.; Wang, D.; Chu, Z.; Lv, Z.; Fan, X. *Coord. Chem. Rev.* **2010**, *254*, 1169.
9. Bernède, J. C. *J. Chil. Chem. Soc.* **2008**, *53*, 1549.
10. Koide, N.; Islam, A.; Chiba, Y.; Han, L. *J. Photochem. Photobiol. A* **2006**, *182*, 296.
11. Longo, C.; Paoli, M.-A. *J. Braz. Chem. Soc.* **2003**, *14*, 889.
12. Xin, X.; Scheiner, M.; Ye, M.; Lin, Z. *Langmuir* **2011**, *27*, 14594.
13. Yoo, B. J.; Lee, D. K. *Polym. Sci. Technol.* **2010**, *21*, 557.
14. Ferber, J.; Luther, J. *Sol. Energy Mater. Sol. Cells* **1998**, *54*, 265.
15. Abdullah, M. H.; Rusop, M. *Ceram. Int.* **2014**, *40*, 967.
16. Hou, R.; Yuan, S.; Ren, X.; Zhao, Y.; Wang, Z.; Zhang, M.; Li, D.; Shi, L. *Electrochim. Acta* **2015**, *154*, 190.
17. Yang, W. G.; Wan, F. R.; Chen, Q. W.; Li, J. J.; Xu, D. S. *J. Mater. Chem.* **2010**, *20*, 2870.
18. Lv, Z.; Fu, Y.; Hou, S.; Wang, D.; Wu, H.; Zhang, C.; Chu, Z.; Zou, D. *Phys. Chem. Chem. Phys.* **2011**, *13*, 10076.
19. Ma, T.; Fang, X.; Akiyama, M.; Inoue, K.; Noma, H.; Abe, E. *J. Electroanal. Chem.* **2004**, *574*, 77.
20. Saito, Y.; Kubo, W.; Kitamura, T.; Wada, Y.; Yanagida, S. *J. Photochem. Photobiol. A* **2004**, *164*, 153.
21. Fang, X.; Ma, T.; Guan, G.; Akiyama, M.; Kida, T.; Abe, E. *J. Electroanal. Chem.* **2004**, *570*, 257.
22. Yoon, C. H.; Vittal, R.; Lee, J. W.; Chae, W. S.; Kim, K. *J. Electrochim. Acta* **2008**, *53*, 2890.
23. Huang, S.; Guo, X.; Huang, X.; Zhang, Q.; Sun, H.; Li, D.; Luo, Y.; Meng, Q. *Nanotechnology* **2011**, *22*, 315.